Experimental study of the influence of hydrogen as a fuel additive on the formation of soot precursors and particles in atmospheric laminar premixed flames of methane

Hong-Quan Do, Luc-Sy Tran, Laurent Gasnot, Xavier Mercier*, Abderrahman El Bakali*

Univ. Lille, CNRS, UMR 8522 - PC2A - Physicochimie des Processus de Combustion et de l'Atmosphère, F-59000 Lille, France

* Corresponding authors:

Prof. Dr. Abderrahman El Bakali, Email: abderrahman.el-bakali@univ-lille.fr

Dr. Xavier Mercier, Email: xavier.mercier@univ-lille.fr

Abstract

We report here the experimental investigation of lightly sooting methane premixed flames with and without hydrogen. Two different approaches were considered to introduce hydrogen in the methane flame, either by keeping the total gas flow rate constant or not. Speciation data were obtained using a set of analytical tools including Gas Chromatography, Fourier-Transform Infrared Spectroscopy, Jet-Cooled Laser-Induced Fluorescence, Laser-induced Incandescence coupled with Cavity Ring-Down Spectroscopy.

The results include mole fraction profiles of gaseous species (C_0-C_{16}) and soot volume fraction (f_v) measured in all studied flames. These results demonstrate that the introduction of hydrogen to the flame insignificantly impacts the maximum mole fractions of small species ($<C_6$) while it strongly influences the concentration of aromatics and f_v. Interestingly, this influence is different, depending on how hydrogen was added to the reference methane flame. An excellent linear relationship between pyrene squared concentration $[C_{16}H_{10}]^2$ and f_v is demonstrated in all investigated flames. Moreover, hydrogen addition changes the slope of these data indicating a non-negligible impact of hydrogen on the rate of the soot nucleation process. These data and the observed linearity between f_v and $[C_{16}H_{10}]^2$ supports therefore the idea of a soot nucleation step initiated by a dimerization process implicating moderate-size polyaromatic hydrocarbons (PAHs) as pyrene. Finally, we note that PAH mole fractions at the beginning of soot formation highlight similar values regardless the flame conditions, which suggests that the inception of the soot formation might be dependent of a minimum concentration threshold of aromatic precursors required to initiate the soot nucleation process.

Keywords: Hydrogen; Methane; Premixed flame; PAHs; Soot nucleation; Soot

1. Introduction

Energy is necessary for almost all industrial and domestic activities and around 80% of the primary energy currently used in the world comes from fossil fuels [1,2]. The world energy demand is growing around 2.3% per year. This increasing energy consumption not only contributes to pollution and environmental deterioration but also to the global warming and climate change mostly due to CO_2 emissions [3,4]. Furthermore, concomitant formation of carbon monoxide (CO), polycyclic aromatic hydrocarbons (PAHs) and soot particles in real combustion processes (especially those involving fuel-rich mixtures), severely affect the human health by damaging the cardiovascular system, weakening the immune system and impairing the lung functions [5,6].

These challenges have motivated researchers to investigate environmentally friendly alternative fuels. In that context, hydrogen (H_2) is emerging as a zero-carbon energy source with low ignition energy, large flammable range and high burning velocity [7–9]. Mixtures of H_2 with natural gas, primarily consisted of methane (CH_4), usually called "hydrogen-enriched natural gas" (HENG), are low-carbon fuel mixtures and being proposed as promising alternative fuels in automotive engines, gas turbines as well as industrial and domestic flame burners [10–15]. To support the development of clean and efficient HENG energy systems, fundamental studies are particularly important, notably to improve our knowledge regarding the co-combustion properties of H_2 and CH_4. Hence, some studies were previously carried out regarding the influence of H_2 as a fuel additive on the global combustion properties of CH_4. For example, the local flame extinction, combustion stability and power output of CH_4 combustion were found to be improved with H_2 enrichment [16,17]. Moreover, it has been demonstrated that the thermal and chemical effects of H_2 addition increased significantly the flame dynamics and combustion efficiency of premixed CH_4 flames [18,19]. Furthermore, the adding of high fraction of H_2 to a CH_4 flame has been shown to exponentially increase the laminar burning velocity [20].

The impact of H_2 on the formation of soot precursors and soot particles have also been the subject of numerous fundamental studies but mostly for mixtures of H_2 with fuels other than CH_4 [21–37]. By contrast, only a few similar studies, to the best of our knowledge, were addressed to characterize the impact of H_2 on the combustion of CH_4 flames [38–41]. Liu *et al.* [38] and Xu *et al.* [39] studied the effects of H_2 as a fuel additive (up to 40% comparing to the base fuel) on soot formation in diffusion CH_4 flames and showed that the addition of H_2 strongly decreases the formation of soot. Ezenwajiaku *et al.* [41] also investigated the impact of H_2 (added up to 20% in CH_4) on the formation of PAHs also in a diffusion flame. The authors studied the formation of PAHs by recording their Laser Induced Fluorescence (LIF) signals collected in the wavelength range 420-480 nm after 283 nm excitation. The measured LIF signal was attributed in this work to the global contribution of PAHs constituted of 3-5 aromatic rings. The authors found this way that the use of H_2 as a fuel additive decreased the amounts of such classes of PAHs. However, those experiments did not enable the selective identification of these PAHs. Mze Ahmed *et al.* [40] experimentally and numerically studied the impact of added H_2 (40% in CH_4) in a premixed laminar sooting flame of methane (equivalence ratio relative to CH_4 Φ_C=2.2) and found that the presence of H_2 in the mixtures promoted the formation of aliphatic C_1-C_4 species as well as benzene and toluene.

However, besides these few reported works, we note that significant specific experimental data listed below are missing in the literature regarding the formation of PAHs and soot in H_2/CH_4 mixture flames. First, no study has ever been published reporting experimental quantification of *individual PAHs* such as naphthalene and pyrene in H_2/CH_4 mixture flames,

while these compounds are expected to be key species in the soot formation process. Second, species profiles determined at *soot nucleation conditions* in H_2/CH_4 mixture flames have never been reported either, while such data are crucial for validating kinetic models and investigating the influence of H_2 in the soot nucleation process. Finally, systematic studies reporting experimental concentration profiles of both gaseous species and solid particles in flames of H_2/CH_4 mixtures remain very scarce while they are of high value to improve our understanding of the co-combustion process of these two fuels and related emissions of PAH and soot.

Hence, the main objective of this reported work is to fill in this gap and shed new light on the role of H_2 in the soot formation, with a specific focus on the soot nucleation process. To this aim, a specific advantage has been taken from the choice of the studied flames, defined as nucleation flames, i.e. flames in which soot only undergoes very slight or even no growth process along the flame height. This property, which can be reached by finely adjusting the equivalent ratio of the flame as explained below, allows the specific study of the nucleation process without being blurred by the growing processes of soot particles that usually take place in standard sooting flames. Two different approaches were employed to introduce H_2 to the reference flame, consisting either in keeping constant or slightly increasing the total flow rate of the gases. Measurements of both gaseous and solid phase species are reported in this work. Hence, profiles of mole fraction species including selected aliphatic and aromatic compounds (C_0-C_{16}) as well as soot volume fractions were obtained using a combination of complementary highly sensitive optical techniques and analytical tools. A discussion is finally proposed regarding the crucial role of H_2 in the nucleation step of the soot formation and hypothetical associated mechanisms implicated in this process.

2. Experimental methods

A laminar premixed flame burner and different experimental techniques were used to carry out this work. These techniques include *(i)* Thermocouple for flame temperature measurement, *(ii)* Gas Chromatography (GC) for the detection of fuel and C_1-C_6 species, *(iii)* Fourier-Transform Infrared Spectroscopy (FTIR) for CO_2 and H_2O profiles, *(iv)* Jet Cooled Laser Induced Fluorescence (JCLIF) for the quantification of PAHs and *(v)* Laser Induced Incandescence (LII) coupled with Cavity Ring-Down Spectroscopy (CRDS) for the measurement of soot volume fraction profiles. These techniques are described in the next sections.

2.1. Burner and flame conditions

Three atmospheric pressure premixed flames were stabilized on a water-cooled McKenna burner with a bronze porous disk (6 cm diameter). The system was already described previously [40]. In the present study, the water-cooling circuit was kept at 296 K and a nitrogen flow, introduced in the co-annular porous of the burner, was set at 1440 NLPH (normal liter per hour) to protect the flame from the perturbation of the surrounding air. The conditions of the studied flames are summarized in Table 1.

Table 1. Experimental conditions. Flame name: Φ-1.82: *CH₄ flame*; Φ-1.82_H₂-S: *CH₄ substituted-H₂ flame*; Φ-1.82_H₂-A: *CH₄ added-H₂ flame*. T_{adia}: adiabatic temperature calculated using GASEQ program [42]. $T_{uncorrected}$: measured temperature by using a type B thermocouple without correction of radiative heat loss. NLPH: normal liter per hour.

	Flame		
	Φ-1.82	Φ-1.82_H₂-S	Φ-1.82_H₂-A
Φ_C	1.82	1.82	1.82
Φ_{C+H}	1.82	1.86	1.86
C/O	0.455	0.455	0.455
Total flow rate (NLPH)	721.4	721.4	734.6
X_{CH4}	0.184	0.184	0.181
X_{O2}	0.202	0.202	0.199
X_{N2}	0.614	0.595	0.602
X_{H2}	0	0.018	0.018
T_{adia} (K)	1820	1821	1805
$T_{uncorrected}$ (K)	1532	1556	1512
Flame speed at 298 K and 1 atm (cm/s)	8.79	9.50	8.82

The premixed CH₄ flame (Φ-1.82) was chosen as the reference flame. This particular flame was defined as a "nucleation" flame, i.e. a flame producing very small amounts of soot particles that do not undergo or very limited surface growth along the height above the burner [43–46]. As previously demonstrated [43,47], soot formation in this kind of flame is dominated by the soot nucleation process while soot growth processes are very limited or efficiently counterbalanced by oxidation or reversible nucleation processes. Therefore, introducing H₂ into such a nucleation flame provides an excellent opportunity to specifically investigate the soot nucleation process involved in the combustion of H₂/CH₄ mixtures and to highlight the influence of H₂ with key species implicated in this process. It is to be noted that the experimental conditions allowing the stabilization of the Φ-1.82 nucleation flame have been determined using the LII technique as described latter in the paper according to a similar protocol used in different recent studies [44–46].

There are currently several approaches to investigate the impact of H₂ in flames. In this work, we defined two different ways of introducing H₂ without significantly affecting the flame burned-gas temperature. The first approach is characterized by a "**H₂ substitution**" and corresponds to the flame Φ-1.82_H₂-S. In this case, a small amount of the nitrogen dilution, equal to 10% of the CH₄ flow rate, is subtracted from the reference flame, and a corresponding amount of H₂ is added to the initial gas flow preserving a constant total flow rate. The second approach corresponds to a "**H₂ addition**" and is denoted as flame Φ-1.82_H₂-A. In this case, a small amount of hydrogen, still equal to 10% of the CH₄ flow rate, is directly added to the initial gas flow, therefore slightly increasing the total flow rate (less than 2%) of the flame compared to that of the reference flame. We admit that these latter conditions are not ideal for identifying a H₂ kinetic effect because the total flow is necessarily modified. However, the main objective of these latter conditions was to generate a different perturbation on the gaseous precursors and soot particles, more specifically at the very beginning of the zone of the soot formation.

Note that these two approaches do not change the initial carbon and oxygen content. The choice of introducing a small amount of H₂ to the reference flame has been made to avoid a significant change of the temperature profiles in the soot formation zone of the different

flames. The gas flow rates were measured by using regulated mass flow controllers (Bronkhorst) with a mass flow accuracy of ±0.5%. The C, O and H balances were checked to be close to 100% as detailed in Table S1 of the Supplemental Material 1 (SM1).

2.2. Analytical techniques

2.2.1. Flame temperature measurements

Flame temperature profiles were measured with a Pt/Rh(6%)-Pt/Rh(30%) type B thermocouple (diameter 100 μm). The thermocouple was coated with a ceramic layer of BeO–Y_2O_3 to reduce catalytic effects [48]. Errors in the peak temperatures were estimated to be ±100 K.

2.2.2. Measurements of gaseous species

2.2.2.1 Gas chromatography (GC):

GC was used to identified and quantify aliphatic species and benzene. The GC and sampling system was previously detailed in [49]. A schematic diagram of the used GC setup is available in SM1 (Fig. S1). Briefly, gas samples were extracted from the flames by a quartz sampling microprobe and then directly sent into a low-pressure injection system connected to the GC CP–3800 Varian. In this experiment, the microprobe (350 μm orifice) was fixed and the burner height was adjustable along the vertical axis, allowing the sampling of species from different heights above the burner. We chose to use this microprobe with a relatively large orifice (350 μm) comparing to usual microprobes generally used for non-sooting flame studies (150 μm) in order to limit the soot clogging issues during the sampling of the species. Moreover, as discussed later, the flames studied in this work generated only small soot particles characterized by small volume fractions (f_v<1x10^{-10}). Hence, our sampling experiments were not affected by clogging problems.

Two columns (a HP-Plot Al_2O_3 Capillary and a Molecular Sieve 5A) and two detectors (a Flame Ionization Detector (FID) and a Thermal Conductivity Detector (TCD)) were used to analyze chemical species sampled from the flames. Gaseous commercial cylinder calibration mixtures (Air Product) with a mole fraction uncertainty of ±0.5–2% have been used to calibrate the GC gaseous species analyzed in the present work. The FID and TCD detection limits were respectively about 0.1 ppm and 10 ppm. The mole fraction uncertainty of gaseous species measured by GC in this study is estimated to be less than ±5% for the major species and ±10% for the minor ones.

2.2.2.2 Fourier-transform infrared spectroscopy (FTIR):

Fourier-transform infrared spectroscopy (FTIR) with a spectrometer NEXUS THERMO-OPTEK was used to measure CO_2 and H_2O mole fractions profiles. The FTIR system was detailed previously in [11,50] and a schematic diagram of this system is available in SM1 (Fig. S2). Gas sample were extracted from the flames using the same microprobe as for GC analyses. The sampling line was heated at 100 °C to avoid water condensation. A rotary valve pump (flow 2.5 m^{3}h^{-1}) allowed the sampling (40 Torr) and conveyed it to a 2-liter heated gas FTIR cell (100 °C) combined with the FTIR apparatus. To avoid the soot deposition on the optical system inside the IRTF gas cell, two filters (QFF, Pall Tissuquartz QAT-UP 2500) were placed before the inlet of the FTIR cell to separate the soot particles from gas sample. The effect of the filters on water condensation was checked. We did not observe any water condensation caused by the use of these filters. The chemical species in the gas sample were analyzed at the time of their passage in the FTIR cell according to an optical path of 10 m. Fifteen scans were realized with

a spectral resolution of 1 cm^{-1}. The FTIR spectra was recorded by OMNIC/QUANTPAD software. The selected spectral zone was chosen at 2394-2276 cm^{-1} for CO_2 measurement and 1719-1698 cm^{-1} for H_2O measurement. The calibration was performed using homemade mixtures of different known compositions of H_2O and CO_2. The uncertainties on CO_2 and H_2O mole fraction were estimated about ±12% and ±11% respectively.

2.2.2.3 Jet Cooled Laser Induced Fluorescence (JC-LIF):

The determination of the mole fraction profiles of two important PAHs (naphthalene and pyrene) has been carried out by Jet Cooled Laser Induced Fluorescence (JCLIF). A schematic diagram of the corresponding experimental setup is shown in SM1 (Figs. S3, S4). The system was previously detailed in [51–53]. Briefly, JCLIF measurements were carried out after the sampling of the species from the flame thanks to the same microprobe as used for the GC experiments. The whole transfer line from the microprobe down to the analysis chamber was kept at quite low pressure (15 Torr) and heated up to 100 °C to limit the condensation of the PAHs [54]. Sampled species from the flame were then directly cooled-down (to around 100 K) inside an expanded free jet generated in a low-pressure analysis chamber. JCLIF measurements were done directly inside the free jet in this chamber. At such low temperature, the spectra of the sampling PAHs simplify and highlight specific spectral structures enabling their selective detection by LIF. In the absence of collisions inside the free jet, LIF signals can then be calibrated by introducing pure PAHs with known concentrations inside the free jet [52,53].

The laser system we used consisted of a Quantel Nd: YAG laser, pumping a dye laser (TDL70 Quantel) with the 2nd harmonic at 532 nm. Two different mixtures of Rhodamine 640 and DCM solved in ethanol were used for the oscillator and amplifier of the dye laser to generate by frequency doubling, a laser pulse tunable either in the wavelength range 300-315 nm or 315-340 nm. The first dye mixture was used to selectively excite the naphthalene species around 308.2 nm [54] while the second dye mixture was used to excite the pyrene molecules around 321 nm [52]. The laser beam was spatially reduced to a diameter of approximately 1 mm with a system of two pinholes and slightly focus into the center of the analysis chamber with a converging lens (f=50cm). The energy was adjusted around 1 mJ/pulse to be in the linear regime of fluorescence. Fluorescence emission spectra were recorded via an imaging spectrometer (Horiba iHR320 - 300 mm focal length - gratings with 300 gr mm^{-1}) which can be coupled either to a 16–bit intensified charge coupled device camera (Roper Pimax II) or a photomultiplier (Photonis XP2020Q). The conditions of excitation and collection wavelengths for the present measurement of naphthalene and pyrene are summarized in Table S2 (SM1). The uncertainty in naphthalene and pyrene mole fraction was estimated around ±13%.

2.2.3. Soot species measurements:

2.2.3.1 Laser Induced Incandescence (LII):

Laser Induced Incandescence (LII) was used in this work for two different purposes, which was *(i)* the identification of the "nucleation flame" conditions and *(ii)* the determination of the soot volume fraction profiles in the different flames. A schematic of the LII setup we used for this study is reported in SM1 (Fig. S5). The system was previously detailed in [44,45] and will be only briefly described here. LII experiments have been carried out by using 1064 nm laser excitation wavelength generated by a Nd: YAG (Quantel) at 10 Hz to heat the soot particles. 1064 nm laser excitation wavelength was used to avoid the excitation of PAHs also formed in

the flames [55]. The laser beam was expanded into a collimated horizontal plane using two cylindrical lenses ($f_1 = -50$ mm, $f_2 = 200$ mm) and then passed through a rectangular slit (5.96 mm (vertical) × 0.61 mm (horizontal)) and a converging lens ($f_3 = 200$ mm) in order to provide a top-hat irradiance profile at the position of the LII collection volume. During these experiments, the laser energy was continuously monitored with a powermeter located after the burner. The LII signal was collected at right angle of the laser axis with two converging lenses ($f_4 = 25$ cm and $f_5 = 20$ cm) and focused on the collection slit (0.6 mm (vertical) × 6 mm (horizontal)). LII signals were measured after the collection slit by a photomultiplier Hamamatsu R2257 (PMT). An interference filter centered at 532 ±9.8 nm was positioned in front of the PMT in order to limit parasite emission and scattering light from the flame. The LII signals recorded by the PMT were acquired and digitized by an oscilloscope Lecroy HDO - 4104A. Before the determination of the LII profiles, fluence curves were determined for different heights above the burner by recording the evolution of the collected LII signal vs laser energy. From these data, a laser fluence of 0.415 J cm^{-2}, *i.e.* under the soot sublimation threshold, was chosen for the measurement of the LII profiles.

2.2.3.2 Cavity Ring-Down Spectroscopy (CRDS):
The LII profiles were then calibrated into soot volume fraction profiles by an extinction measurement carried out by CRDS. To this aim, the soot absorption function E(m) was chosen equal to a constant value of 0.25 as previously determined for nascent soot particles studied in comparable nucleation flames [56]. A schematic diagram of this system is available in SM1 (Fig.S6). The flame was positioned at the center of cavity. The CRDS experiments have been carried out by using a 1064 nm laser excitation wavelength generated by a Nd: YAG (Quantel) at 10 Hz to avoid absorption from gaseous PAHs formed in the flames. The laser beam was shaped to match the TEM$_{00}$ traverse electromagnetic mode of the cavity thanks to two converging lenses with similar focal length (f=10 cm) and a set of two pinholes. The CRDS cavity consisted of two identical 25-mm-diameter plano-concave mirrors (radius of curvature: 25 cm, separated by distance of 40cm, coated to achieve a high reflectivity of R = 99.96% at 1064nm). The laser beam diameter was estimated to be around 300μm and nearly constant along the flame diameter. The light transmitted by the second mirror was collected by a photomultiplier Hamamatsu R2257. A filter RG 780 was placed in front of the PMT to limit the background emission from the flame. The signals were acquired and digitized by an oscilloscope Lecroy HDO - 4104A. The experimental signal was exponentially fitted by a homemade Labview routine to determine the lifetime of the pulse inside the cavity. The uncertainty regarding the soot volume fraction was estimated to be about ±21% in the soot starting zone and ±8% in the post flame region.

3. Results and discussion
The impact of H$_2$ on temperature and major species (*i.e.* fuel, O$_2$, CO, CO$_2$, H$_2$, H$_2$O) are addressed in Sections 3.1 and 3.2, respectively. This impact on soot precursors (C$_2$-C$_{16}$ species) and soot particles (LII decay time, first appearance of the nascent soot particle, relationship between PAHs and nascent soot particles) is discussed in Sections 3.3 and 3.4, respectively.

3.1. Impact of hydrogen on flame temperature
Figure 1 shows the experimental uncorrected temperature profiles of the three studied flames (Φ-1.82, Φ-1.82_H$_2$-S, and Φ-1.82_H$_2$-A). The substitution of hydrogen (Φ-1.82_H$_2$-S) leads to a shift of the temperature profile towards the burner surface, while the addition procedure

(Φ-1.82_H₂-A) does not cause any shift. In both approaches, the maximum temperature is almost similar for the three flames, indicating an insignificant influence of the added H₂ on this flame parameter. Indeed, the maximum temperature of the Φ-1.82_H₂-S and Φ-1.82_H₂-A flames only differs from the reference flame by about 20 K. The temperature is almost identical in the post flame zone of the three studied flames. The adiabatic temperature calculated using GASEQ program [42] confirms the weak impact of H₂ on the flame temperature profiles as shown in Table 1.
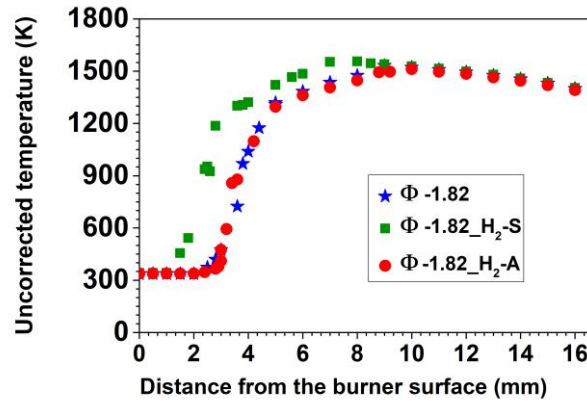
Fig. 1. Impact of hydrogen on flame temperature profiles. Φ-1.82: *CH₄ flame*; Φ-1.82_H₂-S: *CH₄ substituted-H₂ flame*; Φ-1.82_H₂-A: *CH₄ added-H₂ flame* (see Table 1 for the flame conditions).

3.2. Impact of hydrogen on major species (reactants and combustion products)

Figure 2 presents the mole fraction profiles as a function of the distance from the burner surface of the main species including reactants (fuel, O_2) and final products (CO, CO_2, H_2, H_2O) for the three studied flames.
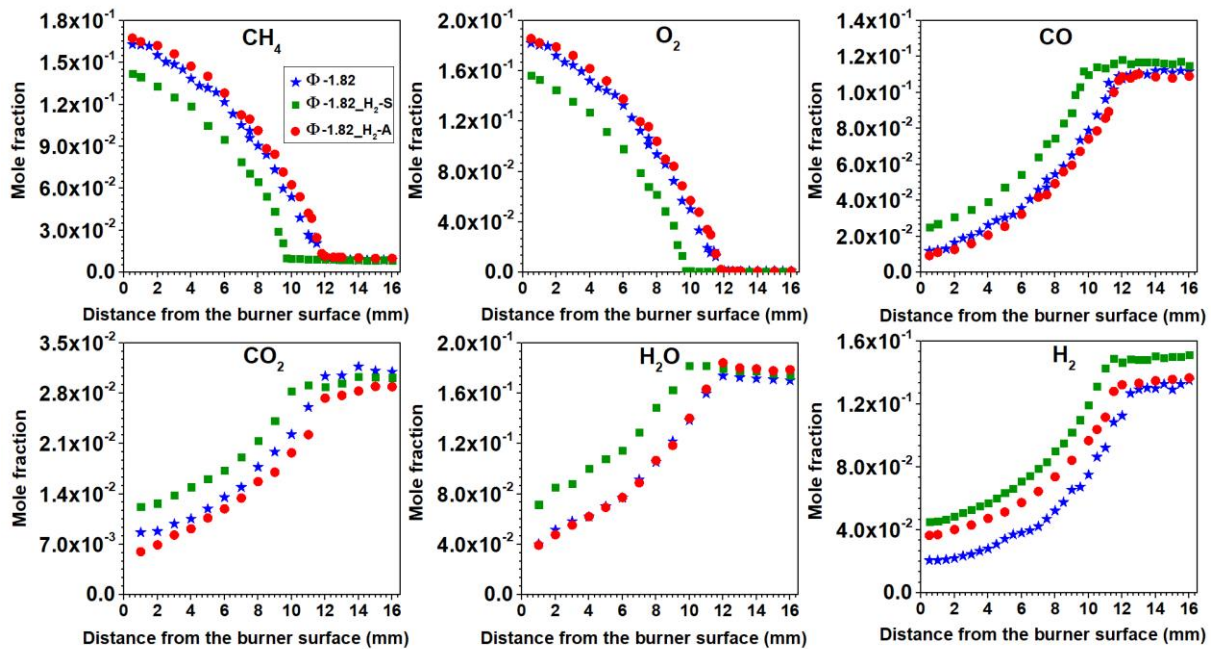

Fig. 2. Mole fraction profiles of reactants (fuel, O_2) and major products (CO, CO_2, H_2, H_2O) as a function of the distance from the burner surface, obtained in the three studied flames.
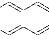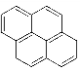
As observed for the temperature profiles reported above, the H_2 substitution (Φ-1.82_H₂-S) systematically shifts the profiles of the major species around 2 mm closer to the burner surface while the H_2 addition (Φ-1.82_H₂-A) does not significantly modify the flame position.

This shift can be attributed to the laminar flame speed increase in the case of H_2 substitution (Φ-1.82_H_2-S). Indeed, according to our calculations carried out for the studied conditions using the GRI mechanism [57], the laminar flame speed of the flame Φ-1.82_H_2-S has been determined around 9.50 cm s^{-1}. This value is actually slightly higher than the flame speed determined for the reference flame speed (8.79 cm s^{-1}) which is very close to the calculated flame speed of the Φ-1.82_H_2-A flame (8.82 cm s^{-1}). As expected, the consumption rate of CH_4 does not nearly evolve anymore beyond 10 mm in the flame Φ-1.82_H_2-S and beyond 12 mm for the two other flames, while O_2 is completely consumed above these distances. Thus, the reaction zone in which the fuel gradually decomposes and the combustion intermediates actively react with each other is located before these distances. The post-flame zone starts just after the reaction zone where the final products (CO, CO_2, H_2, H_2O) become the dominant species in this region. The formation of CO, CO_2, H_2 and H_2O is consistent with the consumption of the fuel and O_2. Indeed, mole fractions of CO, CO_2, H_2 and H_2O expectedly increase in the reaction zone until maximum values reached in the post-flame zone. The slightly higher values of the mole fractions of these products in the reaction zone of the flame Φ-1.82_H_2-S in comparison with the other flames, are explained by the slight shift of the flame front closer to the burner surface. However, the impact of this shift only induces minor changes (within 5%) of the mole fractions of CO, CO_2, and H_2O in the post-flame zone between the different flames.

3.3. Impact of hydrogen on soot precursors

Hydrocarbon species from C_2 to C_{16} corresponding to molar masses ranging from 26 to 202 were identified and quantified with maximum mole fractions comprised between 10^{-2}-10^{-8} and peak position located between 7.5 and 12.5 mm above the burner. The whole species we detected in the three studied flames associated with their chemical structures, maximum mole fractions and peak positions are reported in Table 2. It is to be noted that the sensitivity of the experimental analysis method used for PAH measurements enabled the detection of these species until very low concentrations estimated around the ppb level for pyrene.

Table 2. Nomenclature, name, and structure of soot precursors in the studied flames together with their measured maximum mole fractions x_{max}. DFBS: distance from the burner surface at x_{max} (mm).

Nomenclature	Name	Structure	Flame Φ-1.82		Flame Φ-1.82_H$_2$-S		Flame Φ-1.82_H$_2$-A	
			x_{max}	DFBS (mm)	x_{max}	DFBS (mm)	x_{max}	DFBS (mm)
C_2H_6	Ethane	H_3C—CH_3	6.62×10^{-4}	9.5	7.30×10^{-4}	7.5	6.90×10^{-4}	10.0
C_2H_4	Ethylene	H_2C=CH_2	1.57×10^{-3}	10.0	1.67×10^{-3}	7.5	1.74×10^{-3}	10.0
C_2H_2	Acetylene	HC≡CH	1.17×10^{-2}	11.8	1.21×10^{-2}	9.7	1.30×10^{-2}	11.8
C_3H_8	Propane	H_3C CH_3	1.31×10^{-5}	11.2	1.66×10^{-5}	9.2	1.32×10^{-5}	11.5
C_3H_6	Propene	H_2C CH_3	2.21×10^{-5}	8.5	2.35×10^{-5}	7.5	2.45×10^{-5}	9.0
AC_3H_4	Allene	H_2C CH_2	4.66×10^{-5}	11.2	4.50×10^{-5}	9.5	4.93×10^{-5}	11.5
PC_3H_4	Propyne	HC CH_3	1.11×10^{-4}	11.4	1.07×10^{-4}	9.5	1.20×10^{-4}	11.5
1-C_4H_8	1-Butene	H_3C CH_2	3.00×10^{-6}	11.5	3.28×10^{-6}	9.2	3.34×10^{-6}	11.5
$1,3$-C_4H_6	1,3-Butadiene	H_2C CH_2	6.74×10^{-6}	10.0	6.54×10^{-6}	7.5	7.29×10^{-6}	10.5
BC_4H_6	1-Butyne	H_3C CH	1.94×10^{-5}	11.5	1.87×10^{-5}	9.5	2.25×10^{-5}	11.8
C_6H_6	Benzene		2.10×10^{-5}	11.4	1.72×10^{-5}	9.0	3.13×10^{-5}	11.8
$C_{10}H_8$	Naphthalene		1.54×10^{-6}	11.5	1.01×10^{-6}	9.0	3.09×10^{-6}	11.5
$C_{16}H_{10}$	Pyrene		3.97×10^{-8}	12.0	2.21×10^{-8}	9.5	9.10×10^{-8}	12.5

The impact of hydrogen on the formation of the measured species can be clearer appreciated in Fig. 3 where we have reported the normalized maximum mole fractions, species by species, measured in the three flames. As can be seen in this figure, the introduction of H$_2$ either by addition or substitution, does not significantly influence the maximum mole fractions of the measured aliphatic species. By contrast, it strongly impacts the peak mole fractions of the measured aromatic species (benzene, naphthalene and pyrene), indicating a strong interaction of H$_2$ chemistry with the formation of these aromatic species. This point will be discussed in detail in the following.
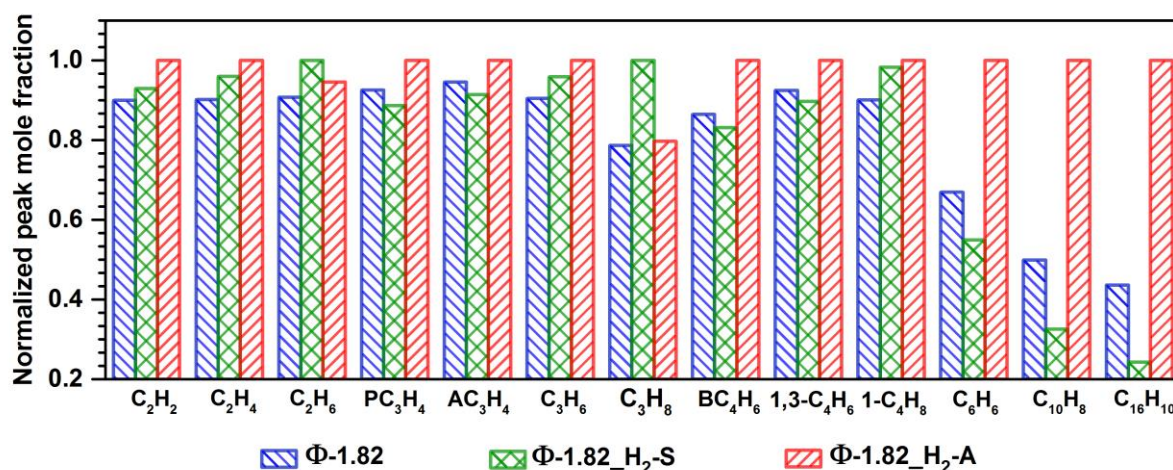

Fig. 3. Graphical summary of the normalized maximum mole fractions of the soot precursors measured in the three studied flames. Normalization has been performed, species by species, regarding to the highest mole fraction value measured in the three flames.

Selected mole fraction profiles of aliphatic and aromatic species measured in the three flames as a function of the distance from the burner surface are presented in Figs. 4 and 5. Figure 4 presents the mole faction profiles of acetylene (C_2H_2), propyne (PC_3H_4) and 1-butyne (BC_4H_6) which are the most abundant species in their corresponding aliphatic group, i.e. characterized by a same carbon number. The mole fraction profiles of other aliphatic species are also available in SM1 (Fig. S7). From this figure, we note that the profiles of the species measured in the flame Φ-1.82_H_2-S are systematically shifted towards the burner surface, consistently with the fuel consumption behavior. However, the introduction of H_2 highlights no significant effect on the shape of the profile and the maximum mole fraction as mentioned earlier. In the present study, only 10% H_2 compared to the fuel was introduced in the flame in order to limit its impact on the temperature profile and allows thus to "selectively" investigate the influence of H_2 on the involved species in the formation of soot particles.
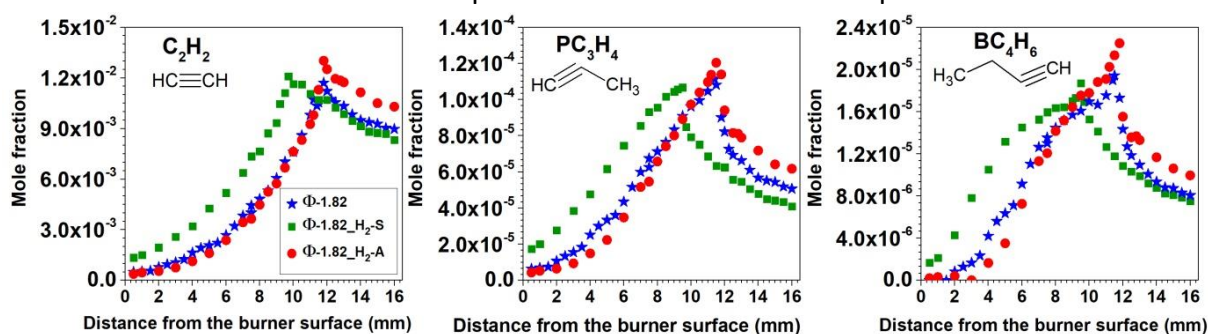

Fig. 4. Mole fraction profiles of selected aliphatic species considered as soot precursors: acetylene, propyne and 1-butyne obtained in the three studied flames.
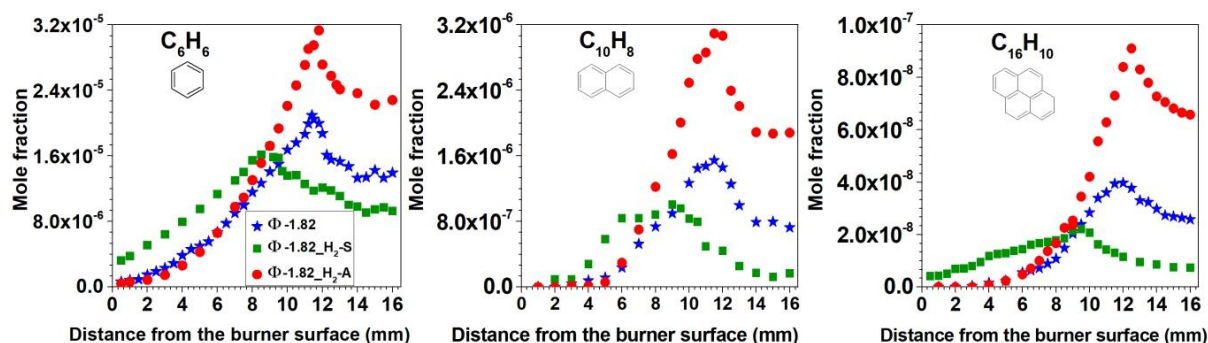

Fig. 5. Mole fraction profiles of benzene, naphthalene and pyrene obtained in the three studied flames.

Figure 5 presents the measured mole fraction profiles of benzene (C_6H_6), naphthalene ($C_{10}H_8$), and pyrene ($C_{16}H_{10}$) which are aromatic species considered as important soot precursors. As can been in this figure, the mole fraction profiles of these species are significantly impacted by H_2 introduction. Moreover, these data show that the impact of H_2 depends on the molar mass of the aromatic compounds. The larger the size of the PAHs, the greater the H_2 effect. It is important to note that the H_2 substitution (Φ-1.82_H_2-S) presents an inhibitory effect (20-50%) on the formation of benzene, naphthalene, and pyrene while the H_2 addition (Φ-1.82_H_2-A) clearly promotes the formation of these aromatics (30-60%). To explain such antagonistic effects, Fig. 6 presents possible competitive processes that share H atoms as reactant. In flame conditions, H_2 can be converted to H atoms mainly by

H2+OH→H+H2O and H2+O→H+OH. The reaction H2+M→H+H+M can also contribute to this conversion in the post flame region. As can be seen from Fig. 6, the branching reaction (path A) competes with the benzene/PAH accumulation process (path B) and the PAH growth processes (path C). Paths D and E are related to soot particles and will be discussed in the next section.
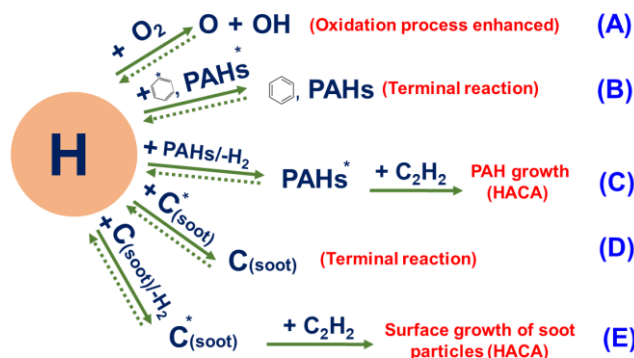

Fig. 6. Possible chemical paths characterizing the kinetic impact of hydrogen atoms in sooting flames. Species written with a star are radicals.

We have shown that H atoms reinforced by the presence of H_2 in the case of substitution essentially serve the reaction (A). This leads to an increase of the laminar flame speed. In other words, H atoms are mainly converted to O and OH radicals under these conditions, resulting in accelerated oxidation processes of aromatic species and in a decrease of H atoms available for processes (B) and (C). These two points explain the decrease of aromatic species mole fraction analyzed under these conditions. In the case of the addition of hydrogen, the reaction (A) is not favored. This is confirmed by the flame front position and by the calculated laminar flame speed of both flames which are similar as reported in Table 1. Thus, H atoms from hydrogen addition sources would benefit primarily for processes (B) and (C). These processes naturally promote a greater formation of benzene and PAHs, giving a soot precursor promoting role to hydrogen under these conditions.

Regarding the well-known and commonly used HACA mechanism, the growth process of PAHs is based on an overall consecutive reaction sequence that begins from the first aromatic ring. This growth process requires acetylene and numerous H-abstraction reactions from PAHs mainly by H atoms. Therefore, in both cases (substitution or addition) the main factors that could explain the important differences regarding the PAHs formation might be the temperature, concentration of H atoms, benzene and acetylene. The analysis of our experimental data allows us to exclude the effect of temperature and acetylene concentration. The effect of H_2 is almost negligible on these two parameters. On the other hand, the recombination of H and phenyl radicals (B) takes a very important role in aromatic species formation in the post flame region as shown in our previous work [58]. The balance of power between A and B processes can be considered at the origin of the experimental PAH observations under the different conditions of the present investigation. Given the high endothermicity of the H elimination from benzene reaction, the B process works in favor of the first aromatic cycle formation. This reaction is very sensitive to the temperature and also to the concentration of H atoms. For example, in the case of H_2 addition, the cumulative effect of the temperature decrease and H concentration increase promotes the recombination reaction of H with the phenyl radicals. Temperature profiles measured in both flames are

substantially identical. So, we can conclude that the observed different impacts on the PAH formation mainly comes from H atoms. Note that the effect is also noticeable on benzene and therefore on PAH mole fraction from 9 mm. Before this position, the impact is limited because reaction B is not dominant in this zone. Outside the soot area, the main reactions regarding the benzene formation are the self-propargyl recombination and the addition of acetylene on butadienyl radicals.

In summary, the promoting effect (addition) or inhibiting effect (substitution) of hydrogen on PAH formation can be explained by a strong competition between the high temperature branching reaction (A) and the recombination of phenyl radicals with H atoms process (B). The decrease (substitution) or increase (addition) of benzene mole fraction mechanically results in a reduction or increase in PAHs given the crucial role of benzene at the beginning of the HACA sequence governing the growth of PAHs. As the sequence is consecutive, the weaker is the mole fraction of aromatic compound in the reference flame, the stronger the effect of a small variation in benzene is. The effect is therefore logically more important on pyrene than on naphthalene in all studied flames.

It is important to specify here that the effect of H_2 in the case of substitution is clearly chemical and that our results exclude a dilution effect. Indeed, the substitution of H_2 in this flame by an equivalent amount of helium does not lead to any variations of the measured species mole fraction profiles. This point is highlighted in Fig. S8 where we report the mole fraction profiles of benzene and its aliphatic precursors measured in the CH_4 flame with added He compared to the CH_4 reference flame. In the case of addition (Φ-1.82_H_2-A), the replacement of H_2 by an equivalent amount of helium could not be performed in this flame because of the flame instability generated by the higher dilution. Therefore, it has not been possible to check the dilution effect on the mole fraction profiles of the measured species according to this approach (He addition) in the flame Φ-1.82_H_2-A. However, the difference in the dilution ratio between the reference flame Φ-1.82 and the flame Φ-1.82_H_2-A is very small (<2%), suggesting that the H_2 dilution effect is certainly negligible. Therefore, it seems reasonable to consider that the differences observed between mole fraction profiles measured in the reference flame Φ-1.82 and the flame Φ-1.82_H_2-A result from chemical effects due to H_2 addition.

3.4. Impact of hydrogen on the formation of soot particles
3.4.1. Determination of the nucleation flame conditions by LII
The LII technique is a powerful and sensitive technique to study soot particles in flames. Details of the method can be found in numerous papers [56,59–62]. Briefly, the measured LII signal, corresponding to the incandescent emission coming from the heated soot particles by a laser pulse, can be expressed according to the following expression:

$$S_{LII}\left(\lambda_{em}, T_p(t)\right) = 48 \cdot E(m) \frac{\pi^2 \cdot h \cdot c^2}{\lambda_{em}{}^6} \cdot \left[\exp\left(\frac{h \cdot c}{\lambda_{em} \cdot k_b \cdot T_p(t)}\right) - 1\right]^{-1} \cdot f_v \qquad eq.1$$

where $E(m)$ is the absorption function of the particles, T_p the temperature of the heated soot by the laser pulse, c the speed of light, λ_{em} the emission wavelength, k_b the Boltzmann constant, h the Planck constant and f_v the soot volume fraction. This last quantity can be further defined as:

$$f_v = \frac{4}{3} \cdot \pi \cdot r_p^3 \cdot N_p \qquad eq.2$$

where N_p and r_p are respectively the number by unit volume and radius of the soot particles. The LII signal is therefore directly related to the size of the generated soot particles and can be used adequately to determine the conditions of the "nucleation" flame, characterized by an invariance of the temporal decay of the LII signals all along the flame height. Hence, the equivalence ratio enabling the generation of the "nucleation flame" in this work has been obtained by following the evolution of the LII temporal decays along the flame height according to a procedure already described in details elsewhere [44,45]. The relationship between the LII temporal decay and the soot size distribution is quite complex [60,63] and requires the use of specific models to interpret the LII signals in terms of primary particle diameter. However, it has been established that the temporal LII decay time is correlated to the diameter of soot particles [60,63] and that the variation of this decay time might be used to characterize the variation of the soot diameter. The longer the decay time the larger the soot particle diameter. Here, we only focus on the characterization of the influence of H_2 as a fuel additive on the relative size of the soot diameter. The determination of the absolute value of the soot particle diameters which can be obtained by modelling the LII signals, although being an interesting topic, is clearly beyond the scope of this paper and will be dealt in a future dedicated work.

We took here benefit of this technique to determine the conditions of the nucleation flames and to examine the influence of added H_2 on the soot formation. These flame conditions were obtained by adjusting the flow rate of the reactants so that we do not observe any growth of the temporal LII decay time all along the flame height, meaning that the size of the soot particles remain constant regardless the height above the burner. By this way, we defined the equivalence ratio Φ-1.82 as the condition characterizing the reference "nucleation flame" (denoted flame Φ-1.82, see flame conditions in Table 1).
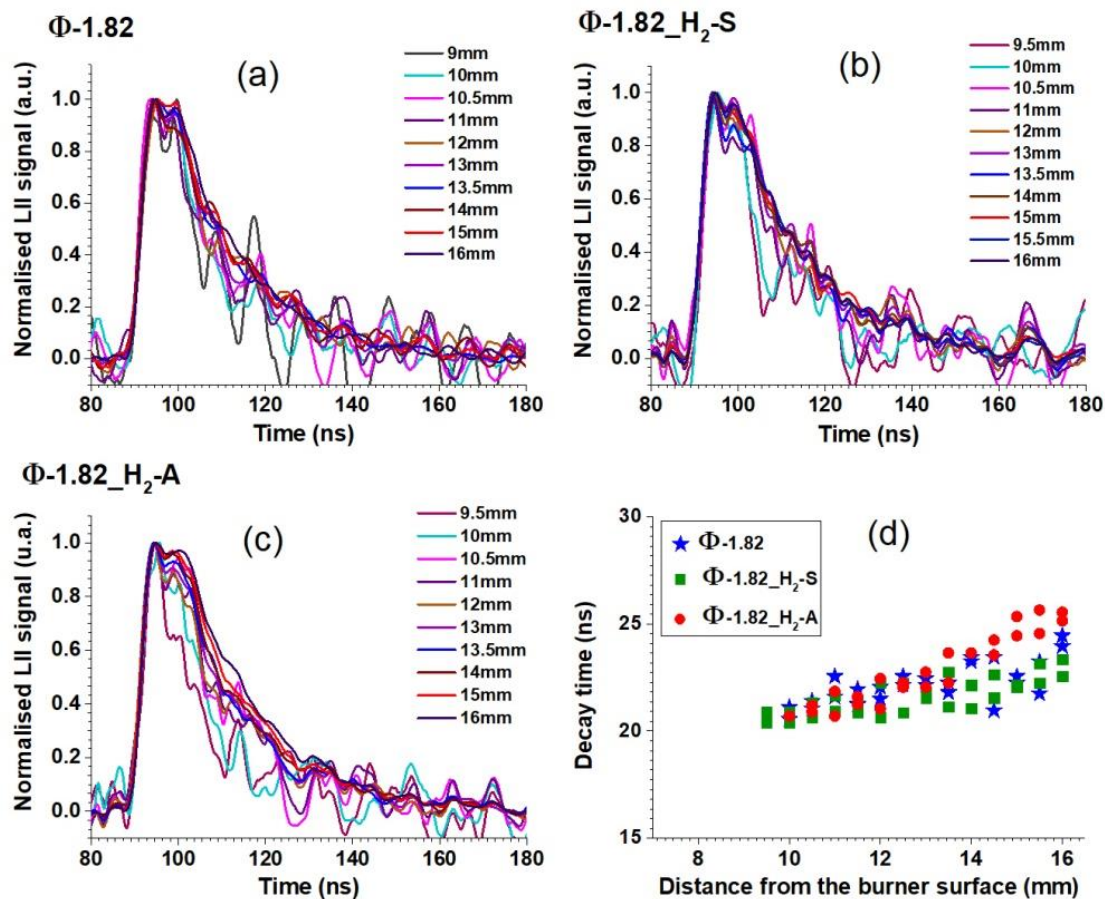
Fig. 7. LII temporal signals measured at different distances from the burner surface in the three studied flames: **(a)** CH$_4$ flame (Φ-1.82), **(b)** CH$_4$ substituted-H$_2$ flame (Φ-1.82_H$_2$-S), **(c)** CH$_4$ added-H$_2$ flame (Φ-1.82_H$_2$-A). For clarity, the peak of LII signals have been normalized to 1. Laser fluence was set at 0.415 J cm^{-2}. **(d)** LII decay-times measured at 1/e of the LII signal as a function of the distance from the burner surface.

The corresponding LII signals according the height above the burner are reported in Fig. 7a, while the determined decay times (corresponding to the time measured at 1/e from the maximum intensity) of these temporal signals are reported in Fig. 7d. Similarly, the temporal LII signals measured in the two flames with added hydrogen, Φ-1.82_H$_2$-S and Φ-1.82_H$_2$-A, are respectively reported in Fig. 7b, c. The corresponding LII decay times for these flames are also reported in Fig. 7d. As can be seen, the introduction of a small amount of H$_2$ in the reference flame does not induce any significant variations the evolution of the LII decays, meaning that the propensity of soot formation of the flames Φ-1.82_H$_2$-S and Φ-1.82_H$_2$-A are close to the one of the "nucleation flame" conditions. This statement is corroborated by the data reported in Fig. 7d, corresponding to the evolution of the LII decay times for the three studied flames. These data highlight a quite constant value of the decay times according to the flame height in the three flames, excepted in the post-flame zone between 14 and 16 mm where we note a slight increase. These data therefore confirm the absence or very weak efficiency of soot growth processes in these three flames, meaning that nucleation is clearly the major process implicated in these flames. It moreover confirms that the small amounts, provided by substitution or addition of H$_2$ to the reference flame, do not significantly influence the size of the soot particles in the early soot formation zone. This property therefore provides a useful opportunity to inspect further the role of the introduced H$_2$ on the formation mechanism of nascent soot particles, as discussed in the next sections.

15

3.4.2. Impact of hydrogen on the appearance of nascent soot particles

Although the mechanism of formation of nascent soot particles from PAHs precursors is still discussed in the community, a large number of studies [43,47,64–69] mentioned that moderate sized PAHs as pyrene could play an important role in the nucleation process. More specifically, the formation of dimers of such PAHs has been suggested as a potential key step allowing the formation of nascent soot particles [47,66–73]. However, because of the weak energy of the Van der Waals bonds characterizing dimers of PAHs, especially at flame temperature [74,75], this hypothesis has often been considered as a numerical tool for kinetic modelling rather than a real physical process actually involved in sooting flames. In that context, Kholghy et *al*. [72] recently suggested a model for the soot nucleation relying on the reversibility of the nucleation process [71,75] associated to the formation of homo and heterogeneous dimers of low molecular weight, stabilized by the formation of a covalent carbon-carbon bound between the two PAHs constituted the dimer. The formation of bonded dimers of moderate-sized PAHs, either by formation of direct covalent bonds or aliphatic bridges, is a current hot topic in the combustion community and has been the subject of different recent experimental and modeling works [68,72,73,76–81]. From these papers, it appears that more and more studies support the idea of a crucial implication of moderate-sized PAHs in the nucleation step leading the formation of the very first particles in flames.

Hence, to further explore this hypothesis and the potential implication of hydrogen in this mechanism, we studied the formation of the very first soot particles formed in our three flames. Figure 8a-c gather the experimental profiles of aromatics (benzene, naphthalene and pyrene) expected to be key species for soot formation. We also report in Fig. 8d the corresponding soot volume fraction profiles measured in each flame. Because of its importance in the analysis of the soot formation, the temperature profiles of the three flames are also added in this figure (Fig. 8e).
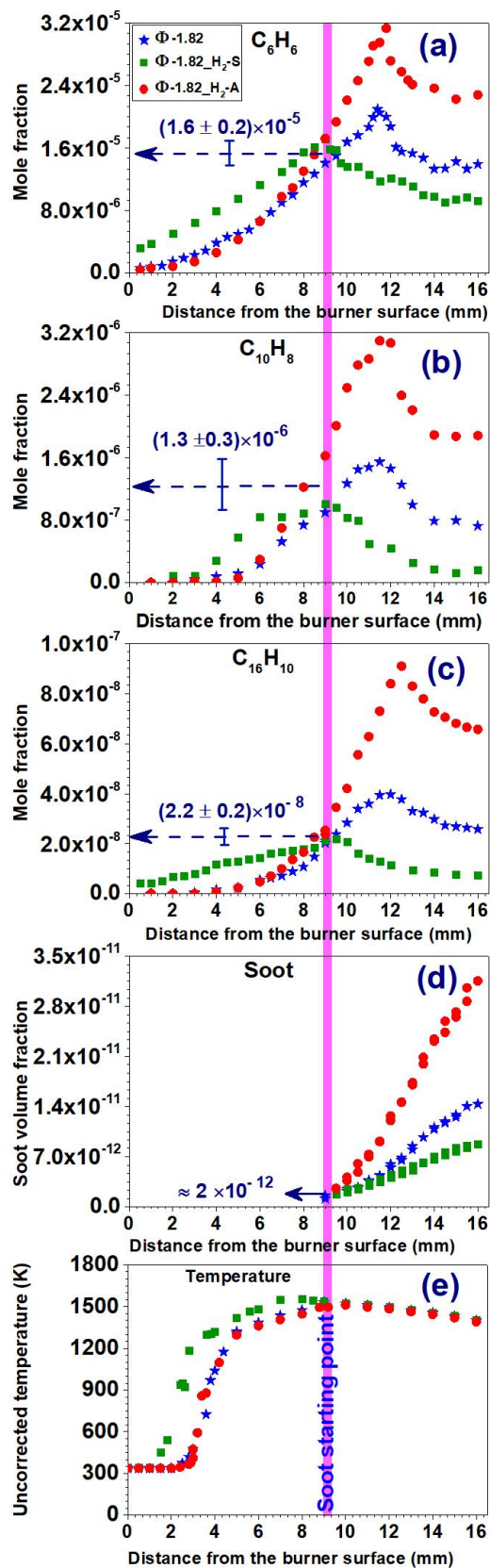
Fig. 8. Profiles of benzene, naphthalene and pyrene mole fraction, soot volume fraction and temperature obtained in the studied flames. The line at 9 mm is drawn to guide the eye regarding the starting point of soot formation.

Several important observations can be drawn from these results. The **first one** concerns the similar trends (increase or decrease) of the PAHs and soot particles maximum values upon H_2 addition or substitution. These data notably show that the formation of soot particles and PAHs are significantly promoted in the flame Φ-1.82_H_2-A while they are strongly inhibited in the flame Φ-1.82_H_2-S (Fig. 8d). Furthermore, the H_2 substitution or addition affects very strongly the PAHs mole fraction in the zone of soot particles formation (Fig. 8a-c). Although this might appear as an expected result, it is important to remind here that we did not observed in these conditions such strong effect on the measured aliphatic precursors as acetylene, propyne, and allene. This experimental observation confirms that aromatic compounds are, much more than aliphatic ones, crucial species in the nucleation process. The role of each aromatic component in the soot nucleation process will be further examined in the next section (Section 3.4.3).

Besides the chemical pathways involving PAHs, a direct influence of the H_2 introduction via the processes (D) and (E) on the concentration of soot particles is not excluded (Fig. 6) although these processes could be less predominant in the early soot nucleation zone [47]. The temperature profiles (Fig. 8e) are quite similar for the three studied flames as discussed earlier. This information is crucial for our further analysis as it guarantees that the differences observed between the soot volume fraction profiles of the three flames are only due to chemical effects related to the introduction of H_2.

The **second observation** which can be made from these data, is the existence of an intercrossing point of the aromatic mole fraction profiles, identified by a pink line in Fig. 8a-c, at a height around 9 mm above the burner, corresponding to the first appearance of the very first particles in each flame. Hence, although H_2 strongly impacts the flame position and the magnitude of the PAH/soot profiles (see Fig. 8a-d), it has no notable influence on the starting point of soot particles profiles. Besides, not only the first soot particles begin to appear at the same height in all these flames but also the corresponding mole fractions of benzene, naphthalene and pyrene measured at this height display very similar values in the three flames, around 1.6×10^{-5} (16 ppm), 1.3×10^{-6} (1.3 ppm), and 2.2×10^{-8} (22 ppb) for benzene, naphthalene and pyrene respectively. Moreover, it is remarkable that the corresponding volume fraction of soot particles determined at 9 mm also highlight a constant value close to $\sim 2 \times 10^{-12}$ ($\sim$2 ppt) in each flame. We precise here that the sensitivity of the LII technique used to carry out these measurements has been demonstrated to be at least 10 times better (around 0.1 ppt) in a previous work [43]. Hence, these data might suggest that the start of the soot formation process might be dependent on specific minimum *concentration "thresholds" of aromatic species,* above only which the nucleation process could take place.

This idea can be rather corroborated by previous measurements of pyrene mole fractions and soot volume fractions made in a methane nucleation flame at low pressure (200 Torr) [43], the profiles of which being reported in Fig. S9. We added on this figure the corresponding species profiles measured in the current atmospheric nucleation flames for comparison. This figure shows that the mole fraction of pyrene measured in the low pressure flame [43] at the very beginning of the soot formation zone reaches a quite similar mole fraction value (~22 ppb) as the one measured here in the atmospheric flames (see Fig. S9).

Much experiments are obviously required to state about this hypothesis of minimum concentration thresholds of aromatics which may be required to enable the soot particle inception to take place. Indeed, although other studies addressed to flames, highlighted properties close to nucleation flames properties exist in the literature, *e.g.* [44,82], no

quantitative profile of aromatics simultaneously measured with soot particles was reported in these works, therefore precluding any further comparisons.

3.4.3. Impact of hydrogen on the soot nucleation rate

To complete the above discussion about the likely dependence of the soot starting point to concentration thresholds of PAHs, we attempt in the present section to discuss the role of the measured individual PAHs on the formation process of the "first" soot particles and the influence of H_2 addition in that context.

As discussed above, a large number of studies and recent theories [43,72,73,75,77] suggest that the formation of the first soot particles comes from the dimerization process of moderate-sized PAHs. From an experimental point of view, Mercier *et al* [73] recently highlighted that the laser induced fluorescence signals emitted in the visible range (450-750 nm), commonly observed in the inception region of sooting flames, might very likely characterize the formation of dimers of moderate-sized PAH. Such hypothesis should therefore imply some kinds of proportional relationships between the nascent soot particles number N_p and the concentration of two PAHs, related to the dimer formation.

The net rate of soot formation normally results from the sum of the rates of many processes such as soot nucleation, soot oxidation, soot growth by PAH condensation on soot surface, chemical soot surface growth (HACA mechanism) and soot particle coagulation. Hence, in standard sooting flames, the complexity of this expression does not allow to establish an immediate correlation between gaseous soot precursors and the formed soot particles. The complexity is even greater if one considers the reversibility of the previous processes. The great advantage of the nucleation flame used in the present study is that this kind of flames allows to minimize many of these processes. In this case, the expression of the net soot formation rate is simplified due to the establishment of a balance between the global soot growth rate and the soot oxidation rate [43]. However, as highlighted by the LII results (Fig. 7), this property (balance between the soot growth and oxidation rates) cannot be considered as fully achieved along the flame height, even in a nucleation flame. We indeed showed above that the soot growth process is not completely inactive in our three nucleation flames, mostly in the zone after the peak of PAHs. So, in order to accurately characterize the reactive species and chemical reactions involved in the nucleation process, it is necessary to specifically consider the soot starting zone where only the nucleation process is activated. To this aim, we have chosen the reaction zone located before the peak of the aromatic species for the analysis of the suggested hypothesis related to the soot formation.

As discussed above, the number of particles N_p is related to the soot volume fraction f_v according to the eq. 2. In the reaction zone located before the peak of the aromatic species of the nucleation flame, the value of r_p, corresponding to the soot radius, remains always constant in this height range of the studied flames. Hence the number of particles N_p is in this case directly proportional the values of f_v measured in this work. In order to appreciate the nature of the aromatic precursors involved in the nucleation process, we have reported the evolution of f_v according to the square of the corresponding concentration of aromatics species (homogeneous dimerization) and the evolution of f_v according to the product of the concentrations of two different PAHs (heterogeneous dimerization). These data are presented in Fig. 9 for the reference methane flame (Φ-1.82) and methane H_2-added flame (Φ-1.82_H_2-A). The presented concentration values of benzene, naphthalene and pyrene have been determined from their measured mole fraction profiles and the corresponding temperature profiles.
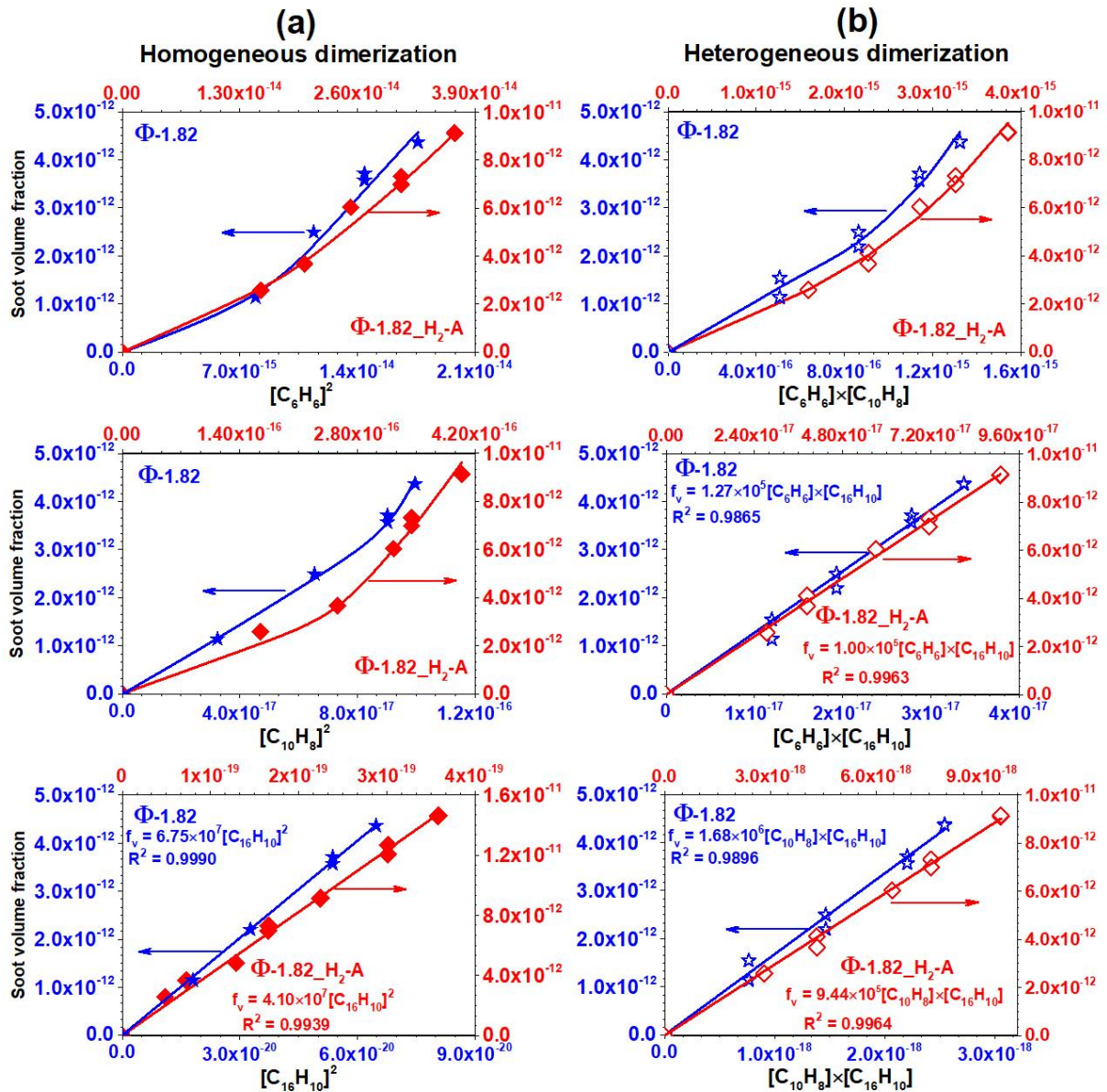
Fig. 9. Influence of H₂ on the relationship between the soot volume fraction and the squared concentration of benzene, naphthalene, and pyrene ($[C_6H_6]^2$, $[C_{10}H_8]^2$, and $[C_{16}H_{10}]^2$) respectively **(a)** and the product of the concentrations of two different PAHs ($[C_6H_6]\times[C_{10}H_8]$, $[C_6H_6]\times[C_{16}H_{10}]$, $[C_{10}H_8]\times[C_{16}H_{10}]$) **(b)** in the soot inception zone of flames Φ-1.82 and Φ-1.82_H₂-A. Flame Φ-1.82: *left and bottom axes*. Flame Φ-1.82_H₂-A: *right and top axes. Symbols:* experiment. *Lines in bottom panel of (a), in middle and bottom panels of (b):* linear fit. *Lines in other panels:* mean curve to guide the eye.

Figure 9a clearly highlights a **direct relationship of proportionality** between pyrene squared concentration ($[C_{16}H_{10}]^2$) and soot volume fraction (f_v) characterized by a linear dependence of these two sets of data in both flames with and without H₂ addition. By contrast, such linear relation is not observed in the case of benzene nor in the case of naphthalene ($[C_6H_6]^2$, $[C_{10}H_8]^2$). The results therefore support this idea of dimerization of moderate sized PAHs as a key step in the soot nucleation process discussed above. Obviously, pyrene might not be the only one species this size implicated in the soot nucleation step. However, the experimental evidence provided here highlights the pertinence of choosing this species in soot

models as a key species to represent the soot nucleation process according to a dimerization process, *i.e.* a process depending on the pyrene-squared concentration [43,47,65,66,83].

Figure 9a also show that **H₂ addition** influences the slope of the regression line characterizing the relationship between $[C_{16}H_{10}]^2$ and f_v. This slope is indeed slightly reduced in the flame Φ-1.82_H₂-A in comparison with the flame Φ-1.82. This reduction therefore denotes a lower formation rate of the nascent soot particles in the flame Φ-1.82_H₂-A, although this flame has been shown to produce more soot than the reference flame (Fig. 8d). The higher total amount of soot produced in the flame Φ-1.82_H₂-A can be easily justified by the higher mole fractions of PAHs formed in this flame.

Assuming that the rate of all the other processes involved in the formation of nascent soot (oxidation of soot, coagulation of nascent soot, condensation of PAHs on the surface of soot, growth in size by chemical reactions of the HACA mechanism, etc.) are unchanged between the flames, the observed reduction of the nucleation rate can be exclusively explained by the effect of hydrogen. If, as suggested by our experimental data, dimerization of pyrene (or other similar sized PAHs) are concerned by the nucleation process, such dimers of moderate-sized PAHs have to be stabilized in order to survive at flame temperature and lead to soot particles. One possibility of stabilization of these dimers would require, as suggested by recent works discussed above, the formation of a chemical bond between the two PAHs constituted the dimer after the physical dimerization (by van der Waals forces). Because this process must release H or H₂, the reversed direction of the process could then be enhanced when adding H₂, thus reducing the soot nucleation rate as observed for the flame Φ-1.82_H₂-A in comparison with the reference flame. The present results therefore support this idea already introduced in the soot formation mechanism developed by Khoghy et *al*. [72].

Finally, it is highly probable, as already said, that heterogeneous dimerization processes implicated pyrene with other PAHs actively participate to the nucleation process. Such mechanisms have notably been proposed in recent kinetic models [72]. This hypothesis has also been considered according to our experimental data by considering different combinations of aromatics to form dimers. These data, corresponding to the products of the considered aromatic concentrations $[C_6H_6]×[C_{10}H_8]$, $[C_6H_6]×[C_{16}H_{10}]$, $[C_{10}H_8]×[C_{16}H_{10}]$ have been reported in Fig 9b according the measured value of f_v in the two flames ⍰-1.82 and Φ-1.82_H₂-A. A linear relationship of proportionality is also observed only when pyrene participates (Fig. 9b, middle and bottom panels). The data therefore strengthen the idea that heterogeneous dimerization processes might play a crucial role, besides homogeneous dimerization, in the soot nucleation process. Moreover, it reinforces the importance of pyrene as a key species in the soot formation models to account for the soot nucleation process.

4. Summary and Conclusion

This paper reports new experimental data obtained in atmospheric "nucleation" flames of methane with and without additional amounts of H₂ (~10% molar). Our results clearly demonstrate the influence of H₂ as a fuel-additive on the formation of soot precursors and first soot particles. These results notably show that the introduction of H₂ strongly influences the concentration of aromatic species and soot, either increases or decreases, according to the operating conditions (addition or substitution of H₂). By contrast, no significant modification was observed regarding the mole fraction profiles of the aliphatic species we measured, even though these species are usually considered as soot precursors as well.

Furthermore, these data also seem to suggest that the inception of the soot particle formation might be controlled by specific concentrations of aromatic precursors, above which the nucleation process can be initiated. This hypothesis is well supported by the measurements of the aromatic concentrations at the very beginning of the soot profiles, characterized by remarkable constant values in all studied flames. These values potentially allowing the inception of the soot formation process have been determined around 16 ppm, 1 ppm and 22 ppb respectively for benzene, naphthalene and pyrene. Although much deeper experiments are required to conclude about these hypothetical threshold values, they have already been highlighted to be consistent with previous experiments carried out in a low-pressure nucleation flame of methane. Such investigations will be the subject of future works by examining whether the existence of these aromatic concentration thresholds are independent of the flame operating conditions and nature of the fuel.

Finally, this work also demonstrates a linear relationship of proportionality between the pyrene squared concentrations and soot volume fractions measured in the inception zone of the soot particles, supporting therefore the hypothesis of pyrene dimerization to describe the nucleation process in soot kinetic models. It is to be noted that the possibility of heterogeneous dimerization of pyrene with benzene and naphthalene has also been checked. Similar linear relationships with soot volume fraction have also been demonstrated in these cases. These results therefore strongly suggest that dimerization, either according homogenous or heterogeneous processes of moderate-sized PAHs, might be the key step governing the soot nucleation process.

These reported data finally constitute a solid database to validate kinetic models of PAHs/soot formation in CH_4/H_2 fuel mixtures. They pave the ways to future studies and further comprehensive modeling analysis to elucidate the role of the identified key species and associated reactions involved in the soot nucleation process.

References
[1]   Zhang X, Zhang M, Zhang H, Jiang Z, Liu C, Cai W. A review on energy, environment and economic assessment in remanufacturing based on life cycle assessment method. J Clean Prod 2020;255:120160. https://doi.org/10.1016/j.jclepro.2020.120160.
[2]   Johnsson F, Kjärstad J, Rootzén J. The threat to climate change mitigation posed by the abundance of fossil fuels. Clim Policy 2019;19:258–74. https://doi.org/10.1080/14693062.2018.1483885.
[3]   Abdin Z, Zafaranloo A, Rafiee A, Mérida W, Lipiński W, Khalilpour KR. Hydrogen as an energy vector. Renew Sustain Energy Rev 2020;120:109620. https://doi.org/10.1016/j.rser.2019.109620.
[4]   Nunes LJR, Causer TP, Ciolkosz D. Biomass for energy: A review on supply chain management models. Renew Sustain Energy Rev 2020;120:109658. https://doi.org/10.1016/j.rser.2019.109658.

[5]   Abdel-Shafy HI, Mansour MSM. A review on polycyclic aromatic hydrocarbons: Source, environmental impact, effect on human health and remediation. Egypt J Pet 2016;25:107–23. https://doi.org/10.1016/j.ejpe.2015.03.011.

[6]   Ghorani-Azam A, Riahi-Zanjani B, Balali-Mood M. Effects of air pollution on human health and practical measures for prevention in Iran. J Res Med Sci 2016;21. https://doi.org/10.4103/1735-1995.189646.

[7]   Lin R-H, Ye Z-Z, Wu B-D. A review of hydrogen station location models. Int J Hydrogen Energy 2020. https://doi.org/10.1016/j.ijhydene.2019.12.035.

[8]   Shen X, Zhang C, Xiu G, Zhu H. Evolution of premixed stoichiometric hydrogen/air flame in a closed duct. Energy 2019;176:265–71. https://doi.org/10.1016/j.energy.2019.03.193.

[9]   Xiao H, Duan Q, Sun J. Premixed flame propagation in hydrogen explosions. Renew Sustain Energy Rev 2018;81:1988–2001. https://doi.org/10.1016/j.rser.2017.06.008.

[10]   Ma F, Wang Y, Liu H, Li Y, Wang J, Zhao S. Experimental study on thermal efficiency and emission characteristics of a lean burn hydrogen enriched natural gas engine. Int J Hydrogen Energy 2007;32:5067–75. https://doi.org/10.1016/j.ijhydene.2007.07.048.

[11]   de Ferrières S, El Bakali A, Lefort B, Montero M, Pauwels JF. Experimental and numerical investigation of low-pressure laminar premixed synthetic natural gas/O2/N2 and natural gas/H2/O2/N2 flames. Combust Flame 2008;154:601–23. https://doi.org/10.1016/j.combustflame.2008.04.018.

[12]   Anandarajah G, McDowall W, Ekins P. Decarbonising road transport with hydrogen and electricity: Long term global technology learning scenarios. Int J Hydrogen Energy 2013;38:3419–32. https://doi.org/10.1016/j.ijhydene.2012.12.110.

[13]   Jones DR, Al-Masry WA, Dunnill CW. Hydrogen-enriched natural gas as a domestic fuel: an analysis based on flash-back and blow-off limits for domestic natural gas appliances within the UK. Sustain Energy Fuels 2018;2:710–23. https://doi.org/10.1039/C7SE00598A.

[14]   Yangaz MU, Özdemir MR, Şener R. Combustion performance of hydrogen-enriched fuels in a premixed burner. Environ Technol 2020;41:2–13. https://doi.org/10.1080/09593330.2019.1656676.

[15]   de Santoli L, Lo Basso G, Barati S, D'Ambra S, Fasolilli C. Seasonal energy and environmental characterization of a micro gas turbine fueled with H2NG blends. Energy 2020;193:116678. https://doi.org/10.1016/j.energy.2019.116678.

[16]   Shen X, Xiu G, Wu S. Experimental study on the explosion characteristics of methane/air mixtures with hydrogen addition. Appl Therm Eng 2017;120:741–7. https://doi.org/10.1016/j.applthermaleng.2017.04.040.

[17]   Zhang C, Shen X, Wen JX, Xiu G. The behavior of methane/hydrogen/air premixed flame in a closed channel with inhibition. Fuel 2020;265:116810. https://doi.org/10.1016/j.fuel.2019.116810.

[18]   Halter F, Chauveau C, Gökalp I. Characterization of the effects of hydrogen addition in premixed methane/air flames. Int J Hydrogen Energy 2007;32:2585–92. https://doi.org/10.1016/j.ijhydene.2006.11.033.

[19]   Hawkes ER, Chen JH. Direct numerical simulation of hydrogen-enriched lean premixed methane–air flames. Combust Flame 2004;138:242–58. https://doi.org/10.1016/j.combustflame.2004.04.010.

[20] Hu E, Huang Z, Zheng J, Li Q, He J. Numerical study on laminar burning velocity and NO formation of premixed methane–hydrogen–air flames. Int J Hydrogen Energy 2009;34:6545–57. https://doi.org/10.1016/j.ijhydene.2009.05.080.

[21] Kumar P, Mishra DP. Experimental investigation of laminar LPG–H2 jet diffusion flame. Int J Hydrogen Energy 2008;33:225–31. https://doi.org/10.1016/j.ijhydene.2007.09.023.

[22] Deng S, Mueller ME, Chan QN, Qamar NH, Dally BB, Alwahabi ZT, et al. Hydrodynamic and chemical effects of hydrogen addition on soot evolution in turbulent nonpremixed bluff body ethylene flames. Proc Combust Inst 2017;36:807–14. https://doi.org/10.1016/j.proci.2016.09.004.

[23] Choudhuri AR, Gollahalli SR. Laser induced fluorescence measurements of radical concentrations in hydrogen–hydrocarbon hybrid gas fuel flames. Int J Hydrogen Energy 2000;25:1119–27. https://doi.org/10.1016/S0360-3199(00)00025-2.

[24] Tesner PA, Robinovitch HJ, Rafalkes IS. The formation of dispersed carbon in hydrocarbon diffusion flames. Symp (Int) Combust 1961;8:801–6. https://doi.org/10.1016/S0082-0784(06)80575-8.

[25] Du DX, Axelbaum RL, Law CK. Soot formation in strained diffusion flames with gaseous additives. Combust Flame 1995;102:11–20. https://doi.org/10.1016/0010-2180(95)00043-6.

[26] Choi J-H, Hwang C-H, Choi SK, Lee SM, Lee WJ, Jang SH, et al. Impacts of hydrogen addition on micro and nanostructure of soot particles formed in C2H4/air counter diffusion flames. Int J Hydrogen Energy 2016;41:15852–8. https://doi.org/10.1016/j.ijhydene.2016.04.158.

[27] Gülder ÖL, Snelling DR, Sawchuk RA. Influence of hydrogen addition to fuel on temperature field and soot formation in diffusion flames. Symp (Int) Combust 1996;26:2351–8. https://doi.org/10.1016/S0082-0784(96)80064-6.

[28] Glassman I. Sooting laminar diffusion flames: Effect of dilution, additives, pressure, and microgravity. Symp (Int) Combust 1998;27:1589–96. https://doi.org/10.1016/S0082-0784(98)80568-7.

[29] Guo H, Liu F, Smallwood GJ, Gülder ÖL. Numerical study on the influence of hydrogen addition on soot formation in a laminar ethylene–air diffusion flame. Combust Flame 2006;145:324–38. https://doi.org/10.1016/j.combustflame.2005.10.016.

[30] Gu M, Chu H, Liu F. Effects of simultaneous hydrogen enrichment and carbon dioxide dilution of fuel on soot formation in an axisymmetric coflow laminar ethylene/air diffusion flame. Combust Flame 2016;166:216–28. https://doi.org/10.1016/j.combustflame.2016.01.023.

[31] Sun Z, Dally B, Nathan G, Alwahabi Z. Effects of hydrogen and nitrogen on soot volume fraction, primary particle diameter and temperature in laminar ethylene/air diffusion flames. Combust Flame 2017;175:270–82. https://doi.org/10.1016/j.combustflame.2016.08.031.

[32] Zhao H, Stone R, Williams B. Investigation of the soot formation in ethylene laminar diffusion flames when diluted with helium or supplemented by hydrogen. Energ Fuel 2014;28:2144–51. https://doi.org/10.1021/ef401970q.

[33] Pandey P, Pundir BP, Panigrahi PK. Hydrogen addition to acetylene–air laminar diffusion flames: Studies on soot formation under different flow arrangements. Combust Flame 2007;148:249–62. https://doi.org/10.1016/j.combustflame.2006.09.004.

[34] De Iuliis S, Maffi S, Migliorini F, Cignoli F, Zizak G. Effect of hydrogen addition on soot formation in an ethylene/air premixed flame. Appl Phys B 2012;106:707–15. https://doi.org/10.1007/s00340-012-4903-2.

[35] Haynes BS, Jander H, Mätzing H, Wagner HGg. The influence of gaseous additives on the formation of soot in premixed flames. Symp (Int) Combust 1982;19:1379–85. https://doi.org/10.1016/S0082-0784(82)80314-7.

[36] Wei M, Liu J, Guo G, Li S. The effects of hydrogen addition on soot particle size distribution functions in laminar premixed flame. Int J Hydrogen Energy 2016;41:6162–9. https://doi.org/10.1016/j.ijhydene.2015.10.022.

[37] Park S-H, Lee K-M, Hwang C-H. Effects of hydrogen addition on soot formation and oxidation in laminar premixed C2H2/air flames. Int J Hydrogen Energy 2011;36:9304–11. https://doi.org/10.1016/j.ijhydene.2011.05.031.

[38] Liu F, Ai Y, Kong W. Effect of hydrogen and helium addition to fuel on soot formation in an axisymmetric coflow laminar methane/air diffusion flame. Int J Hydrogen Energy 2014;39:3936–46. https://doi.org/10.1016/j.ijhydene.2013.12.151.

[39] Xu L, Yan F, Wang Y, Chung SH. Chemical effects of hydrogen addition on soot formation in counterflow diffusion flames: Dependence on fuel type and oxidizer composition. Combust Flame 2020;213:14–25. https://doi.org/10.1016/j.combustflame.2019.11.011.

[40] Mze Ahmed A, Mancarella S, Desgroux P, Gasnot L, Pauwels J-F, El Bakali A. Experimental and numerical study on rich methane/hydrogen/air laminar premixed flames at atmospheric pressure: Effect of hydrogen addition to fuel on soot gaseous precursors. Int J Hydrogen Energy 2016;41:6929–42. https://doi.org/10.1016/j.ijhydene.2015.11.148.

[41] Ezenwajiaku C, Talibi M, Doan NAK, Swaminathan N, Balachandran R. Study of polycyclic aromatic hydrocarbons (PAHs) in hydrogen-enriched methane diffusion flames. Int J Hydrogen Energy 2019;44:7642–55. https://doi.org/10.1016/j.ijhydene.2019.01.253.

[42] Gaseq Chemical Equilibrium Program n.d. http://www.gaseq.co.uk/ (accessed February 28, 2020).

[43] Desgroux P, Faccinetto A, Mercier X, Mouton T, Aubagnac Karkar D, El Bakali A. Comparative study of the soot formation process in a "nucleation" and a "sooting" low pressure premixed methane flame. Combust Flame 2017;184:153–66. https://doi.org/10.1016/j.combustflame.2017.05.034.

[44] Bladh H, Olofsson N-E, Mouton T, Simonsson J, Mercier X, Faccinetto A, et al. Probing the smallest soot particles in low-sooting premixed flames using laser-induced incandescence. Proc Combust Inst 2015;35:1843–50. https://doi.org/10.1016/j.proci.2014.06.001.

[45] Mouton T, Mercier X, Wartel M, Lamoureux N, Desgroux P. Laser-induced incandescence technique to identify soot nucleation and very small particles in low-pressure methane flames. Appl Phys B 2013;112:369–79. https://doi.org/10.1007/s00340-013-5446-x.

[46] Betrancourt C, Liu F, Desgroux P, Mercier X, Faccinetto A, Salamanca M, et al. Investigation of the size of the incandescent incipient soot particles in premixed sooting and nucleation flames of n-butane using LII, HIM, and 1 nm-SMPS. Aerosol Sci Technol 2017;51:916–35. https://doi.org/10.1080/02786826.2017.1325440.

[47] Aubagnac-Karkar D, El Bakali A, Desgroux P. Soot particles inception and PAH condensation modelling applied in a soot model utilizing a sectional method. Combust Flame 2018;189:190–206. https://doi.org/10.1016/j.combustflame.2017.10.027.

[48] Kint JH. A noncatalytic coating for platinum-rhodium thermocouples. Combust Flame 1970;14:279–81. https://doi.org/10.1016/S0010-2180(70)80040-2.

[49] de Ferrières S, El Bakali A, Gasnot L, Montero M, Pauwels JF. Kinetic effect of hydrogen addition on natural gas premixed flames. Fuel 2013;106:88–97. https://doi.org/10.1016/j.fuel.2012.06.045.

[50] Lefort B, El Bakali A, Gasnot L, Pauwels JF. Experimental and numerical investigation of low-pressure laminar premixed synthetic natural gas flames in rich conditions. Fuel 2017;189:210–37. https://doi.org/10.1016/j.fuel.2016.10.043.

[51] Mercier X, Wartel M, Pauwels J-F, Desgroux P. Implementation of a new spectroscopic method to quantify aromatic species involved in the formation of soot particles in flames. Appl Phys B 2008;91:387–95. https://doi.org/10.1007/s00340-008-2997-3.

[52] Mouton T, Mercier X, Desgroux P. Isomer discrimination of PAHs formed in sooting flames by jet-cooled laser-induced fluorescence: application to the measurement of pyrene and fluoranthene. Appl Phys B 2016;122:123. https://doi.org/10.1007/s00340-016-6397-9.

[53] Wartel M, Pauwels J-F, Desgroux P, Mercier X. Pyrene measurements in sooting low pressure methane flames by jet-cooled laser-induced fluorescence. J Phys Chem A 2011;115:14153–62. https://doi.org/10.1021/jp206970t.

[54] Wartel M, Pauwels J-F, Desgroux P, Mercier X. Quantitative measurement of naphthalene in low-pressure flames by jet-cooled laser-induced fluorescence. Appl Phys B 2010;100:933–43. https://doi.org/10.1007/s00340-010-4135-2.

[55] Schoemaecker Moreau C, Therssen E, Mercier X, Pauwels JF, Desgroux P. Two-color laser-induced incandescence and cavity ring-down spectroscopy for sensitive and quantitative imaging of soot and PAHs in flames. Appl Phys B 2004;78:485–92. https://doi.org/10.1007/s00340-003-1370-9.

[56] Betrancourt C, Mercier X, Liu F, Desgroux P. Quantitative measurement of volume fraction profiles of soot of different maturities in premixed flames by extinction-calibrated laser-induced incandescence. Appl Phys B 2019;125:16. https://doi.org/10.1007/s00340-018-7127-2.

[57] Smith GP, Golden DM, Frenklach M, Moriarty NW, Eiteneer B, Goldenberg M, et al. GRI-Mech 3.0, URL: <http://www.me.berkeley.edu/gri_mech> 51; 1999 p.55 n.d.

[58] El Bakali A, Mercier X, Wartel M, Acevedo F, Burns I, Gasnot L, et al. Modeling of PAHs in low pressure sooting premixed methane flame. Energy 2012;43:73–84. https://doi.org/10.1016/j.energy.2011.12.026.

[59] Yon J, Lemaire R, Therssen E, Desgroux P, Coppalle A, Ren KF. Examination of wavelength dependent soot optical properties of diesel and diesel/rapeseed methyl ester mixture by extinction spectra analysis and LII measurements. Appl Phys B 2011;104:253–71. https://doi.org/10.1007/s00340-011-4416-4.

[60] Michelsen HA, Liu F, Kock BF, Bladh H, Boiarciuc A, Charwath M, et al. Modeling laser-induced incandescence of soot: a summary and comparison of LII models. Appl Phys B 2007;87:503–21. https://doi.org/10.1007/s00340-007-2619-5.

[61] Bladh H, Johnsson J, Olofsson N-E, Bohlin A, Bengtsson P-E. Optical soot characterization using two-color laser-induced incandescence (2C-LII) in the soot growth region of a premixed flat flame. Proc Combust Inst 2011;33:641–8. https://doi.org/10.1016/j.proci.2010.06.166.

[62] Liu F, Snelling DR, Thomson KA, Smallwood GJ. Sensitivity and relative error analyses of soot temperature and volume fraction determined by two-color LII. Appl Phys B 2009;96:623–36. https://doi.org/10.1007/s00340-009-3560-6.

[63] Michelsen HA. Understanding and predicting the temporal response of laser-induced incandescence from carbonaceous particles. J Chem Phys 2003;118:7012–45. https://doi.org/10.1063/1.1559483.

[64] Appel J, Bockhorn H, Wulkow M. A detailed numerical study of the evolution of soot particle size distributions in laminar premixed flames. Chemosphere 2001;42:635–45. https://doi.org/10.1016/S0045-6535(00)00237-X.

[65] Lindstedt RP, Waldheim BBO. Modeling of soot particle size distributions in premixed stagnation flow flames. Proc Combust Inst 2013;34:1861–8. https://doi.org/10.1016/j.proci.2012.05.047.

[66] Schuetz CA, Frenklach M. Nucleation of soot: Molecular dynamics simulations of pyrene dimerization. Proc Combust Inst 2002;29:2307–14. https://doi.org/10.1016/S1540-7489(02)80281-4.

[67] Eaves NA, Dworkin SB, Thomson MJ. Assessing relative contributions of PAHs to soot mass by reversible heterogeneous nucleation and condensation. Proc Combust Inst 2017;36:935–45. https://doi.org/10.1016/j.proci.2016.06.051.

[68] Mercier X, Faccinetto A, Batut S, Vanhove G, Božanić DK, Hróðmarsson HR, et al. Selective identification of cyclopentaring-fused PAHs and side-substituted PAHs in a low pressure premixed sooting flame by photoelectron photoion coincidence spectroscopy. Phys Chem Chem Phys 2020;22:15926–44. https://doi.org/10.1039/D0CP02740E.

[69] Faccinetto A, Irimiea C, Minutolo P, Commodo M, D'Anna A, Nuns N, et al. Evidence on the formation of dimers of polycyclic aromatic hydrocarbons in a laminar diffusion flame. Commun Chem 2020;3:1–8. https://doi.org/10.1038/s42004-020-00357-2.

[70] Siegmann K, Sattler K. Formation mechanism for polycyclic aromatic hydrocarbons in methane flames. J Chem Phys 1999;112:698–709. https://doi.org/10.1063/1.480648.

[71] Eaves NA, Dworkin SB, Thomson MJ. The importance of reversibility in modeling soot nucleation and condensation processes. Proc Combust Inst 2015;35:1787–94. https://doi.org/10.1016/j.proci.2014.05.036.

[72] Kholghy MR, Kelesidis GA, Pratsinis SE. Reactive polycyclic aromatic hydrocarbon dimerization drives soot nucleation. Phys Chem Chem Phys 2018;20:10926–38. https://doi.org/10.1039/C7CP07803J.

[73] Mercier X, Carrivain O, Irimiea C, Faccinetto A, Therssen E. Dimers of polycyclic aromatic hydrocarbons: the missing pieces in the soot formation process. Phys Chem Chem Phys 2019;21:8282–94. https://doi.org/10.1039/C9CP00394K.

[74] Sabbah H, Biennier L, Klippenstein SJ, Sims IR, Rowe BR. Exploring the Role of PAHs in the Formation of Soot: Pyrene Dimerization. J Phys Chem Lett 2010;1:2962–7. https://doi.org/10.1021/jz101033t.

[75] Wang H. Formation of nascent soot and other condensed-phase materials in flames. Proc Combust Inst 2011;33:41–67. https://doi.org/10.1016/j.proci.2010.09.009.

[76] Krueger RA, Blanquart G. Predicting aromatic exciplex fluorescence emission energies. Phys Chem Chem Phys 2019;21:10325–35. https://doi.org/10.1039/C9CP02027F.

[77] Martin JW, Hou D, Menon A, Pascazio L, Akroyd J, You X, et al. Reactivity of polycyclic aromatic hydrocarbon soot precursors: implications of localized π-radicals on rim-based pentagonal rings. J Phys Chem C 2019;123:26673–82. https://doi.org/10.1021/acs.jpcc.9b07558.

[78] Johansson KO, Head-Gordon MP, Schrader PE, Wilson KR, Michelsen HA. Resonance-stabilized hydrocarbon-radical chain reactions may explain soot inception and growth. Science 2018;361:997–1000. https://doi.org/10.1126/science.aat3417.

[79] D'Anna A, Violi A, D'Alessio A, Sarofim AF. A reaction pathway for nanoparticle formation in rich premixed flames. Combust Flame 2001;127:1995–2003. https://doi.org/10.1016/S0010-2180(01)00303-0.

[80] Frenklach M, Mebel AM. On the mechanism of soot nucleation. Phys Chem Chem Phys 2020;22:5314–31. https://doi.org/10.1039/D0CP00116C.

[81] Adamson BD, Skeen SA, Ahmed M, Hansen N. Detection of Aliphatically Bridged Multi-Core Polycyclic Aromatic Hydrocarbons in Sooting Flames with Atmospheric-Sampling High-Resolution Tandem Mass Spectrometry. J Phys Chem A 2018;122:9338–49. https://doi.org/10.1021/acs.jpca.8b08947.

[82] Tang Q, Wang M, You X. Measurements of sooting limits in laminar premixed burner-stabilized stagnation ethylene, propane, and ethylene/toluene flames. Fuel 2019;235:178–84. https://doi.org/10.1016/j.fuel.2018.07.090.

[83] Singh J, Balthasar M, Kraft M, Wagner W. Stochastic modeling of soot particle size and age distributions in laminar premixed flames. Proc Combust Inst 2005;30:1457–65. https://doi.org/10.1016/j.proci.2004.08.120.